Journal of Applied Polymer Science

On the use of ball milling to develop poly(3-hydroxybutyrate-co-3-hydroxyvalerate)-graphene nanocomposites (II)—Mechanical, barrier, and electrical properties

Jesús Ambrosio-Martín,[1] Giuliana Gorrasi,[2] Amparo Lopez-Rubio,[1] María José Fabra,[1] Luís Cabedo Mas,[3] Miguel Angel López-Manchado,[4] Jose María Lagaron[1]

[1]Novel Materials and Nanotechnology Group, IATA, CSIC, Av. Agustín Escardino 7 46980 Paterna (Valencia), Spain
[2]Department of Industrial Engineering University of Salerno, Via Giovanni Paolo II 132 84084 Fisciano Salerno, Italy
[3]ESID, Universitat Jaume I, Avda. Vicent Sos Baynat s/n 12071 Castellón, Spain
[4]Institute of Polymer Science and Technology, (CSIC), Juan de la Cierva, 3 28006 Madrid, Spain
Correspondence to: G. Gorrasi (E-mail: ggorrasi@unisa.it) and J. M. Lagaron (E-mail: lagaron@iata.csic.es)

ABSTRACT: In this work, poly (3-hydroxybutyrate-co-3-hydroxyvalerate) (PHBV) nanocomposites containing functionalized graphene sheets (FGS) were prepared by means of high-energy ball milling. The crystalline structure, oxygen barrier, mechanical and electrical properties, and biodegradability of the developed nanocomposites were analyzed and correlated with the amount of FGS incorporated and with their morphology, which was reported in a previous study. Addition of FGS into the PHBV matrix did not affect the crystal morphology of the material but led to somewhat enhanced crystallinity. The good dispersion and distribution of the nanofiller within the polymeric matrix, revealed in the first part of this study, was thought to be crucial for the mechanical reinforcing effect of FGS and also resulted in enhanced gas barrier properties at high relative humidity. Additionally, the conducting behavior of the nanocomposites, as interpreted by the percolation theory, displayed a very low percolation threshold set at ~0.3 vol % of FGS, while the materials exhibited an overall significantly enhanced conductivity. © 2015 Wiley Periodicals, Inc. J. Appl. Polym. Sci. **2015**, *132*, 42217.

KEYWORDS: biopolymers & renewable polymers; blends; graphene and fullerenes

Received 24 February 2015; accepted 11 March 2015
DOI: 10.1002/app.42217

INTRODUCTION

Great efforts have been focused on the development of environmentally friendly biodegradable polymers in the last decades because of the nonrenewable and nonbiodegradable character of the petroleum-based synthetic polymers, particularly in the packaging area, where a huge amount of plastic waste is generated on a daily basis. Polyhydroxyalkanoates (PHAs) are one of the most studied families of thermoplastic biodegradable polymers not only because of their environmentally friendly properties such as biodegradability, biocompatibility, and renewable character but also because these materials have mechanical properties similar to those of conventional petroleum-based polymers, relatively good thermal properties, melt compounding processability and high stiffness because of its high crystallinity degree.[1] Specifically, poly(3-hydroxybutyrate-co-3-hydroxyvalerate) (PHBV), the copolymers which belong to the PHAs family, have been extensively studied and quickly identified as good candidates to replace fossil-based commodity polymers. However, several properties of these biopolymers, including the mechanical, thermal and barrier properties need to be balanced or improved in order to extend their field of application.[1,2] Among the strategies used to balance these physical properties, the use of organic and inorganic nanofillers as reinforcing agents have been extensively used. For instance, inorganic nanofillers such as carbon nanotubes[3] and nanoclays[4–6] have been used. In the case of organic fillers, cellulose nanocrystals[1,7–9] have been the most widely used material for this purpose.

In last years, graphene, a two-dimensional material consisting of a single layer of carbon atoms packed in a hexagonal lattice, has gained much attention because of its remarkable physical properties such as mechanical, thermal, and electrical properties. Because of that, graphene materials are expected to be used in a variety of applications including sensors, batteries, supercapacitors, active and intelligent packaging devices and hydrogen storage systems.[10]

Out of all the processes for the production of graphene, e.g. mechanical exfoliation, chemical exfoliation, chemical vapor

deposition or epitaxial growth, the reduction of graphene derivatives such as graphene oxide has attracted more attention since it is a route able to produce graphene sheets in both colloidal dispersions and powder forms with high processability. Moreover, the presence of oxygen functionalities in the graphene oxide is very interesting from a chemical point of view. Therefore, graphene derivatives are also expected to serve as reinforcement fillers in nanocomposite materials since they provide reactive sites for chemical interactions with the matrix.[10,11] The most well-known processes to prepare polymer nanocomposites are solution casting, *in situ* polymerization and melt blending.[12,13] Graphene and its derivatives have already been extensively used as reinforcing agents in different polymer and biopolymer matrices such as polyvinyl alcohol (PVA),[14] polyethylene (PE),[15] polyamide-6 (PA6),[16] polystyrene (PS),[17,18] poly (lactic acid) (PLA),[13] and PHBV.[2] In these studies, improved mechanical, thermal, and/or electrical properties were reported. Thus, for example, improvement in Young's Modulus (of up to 10 fold)[19] and in electrical conductivity (up to 13 orders of magnitude)[20] were reported after incorporation of graphene in PVA by solution casting. Similar reinforcing effects, where the storage modulus was seen to increase by up to 118% for PE-nanocomposites obtained by solution casting[21] and 87% and 77% in Young's Modulus and tensile strength, respectively, for those PE-nanocomposites obtained by melt compounding[15] were also reported. Moreover, PE-graphene nanocomposites obtained by *in situ* polymerization showed improvements in thermal stability with an increase in thermal degradation temperature of up to 30°C and in electrical properties of up to nine orders of magnitude.[22] Regarding the use of graphene and its derivatives to reinforce biopolymer matrices, Kim *et al.*[23] prepared polylactide nanocomposites with exfoliated graphite via melt compounding. The thermal stability, mechanical modulus, and electrical conductivity were significantly improved. Pinto *et al.*[24] showed improvements of up to 85% and 15% in Young's Modulus and tensile strength, respectively, after addition of both graphene oxide and graphene nanoplatelets in PLA via solution casting with no differences between both fillers. Moreover, in the work of Shen *et al.*[25] an increased electrical conductivity of up to 15 orders of magnitude, was also reported upon addition of chemically reduced graphene oxide into PLA using the same incorporation route. Although, it is widely known that solution casting leads to a relative good dispersion of graphene within polymeric matrices, a recent study demonstrated that surface modification of graphene oxide by grafting PLA chains prior to the solution casting further enhances the dispersion of the filler and resulted in higher mechanical properties.[26] *In situ* ring opening polymerization has also been used to prepare PLA grafted to thermally reduced graphene oxide (TRG) sheets with improvements of up to 18°C in thermal degradation temperature and up to 12 orders of magnitude in electrical conductivity. An enhanced dispersion was obtained if compared with the materials obtained by melt blending PLA with TRG.[27] In the open literature, there are very few studies reporting on the incorporation of graphene into PHBV. Sridhar *et al.*[2] reported enhancements in mechanical properties and thermal stability of PHBV with improvements in tensile strength (25%), elastic modulus (higher than 100%) and thermal degradation temperature (10°C) after incorporation of 6 wt % of graphene into PHBV by solution casting. Furthermore, Wang *et al.*[28] observed similar effects, with an increase of 18°C on thermal degradation temperature and improvements in the storage modulus in the whole temperature range analyzed. In this case, solution casting was also used to incorporate graphene into PHBV but lower amount of filler, 1wt %, was necessary to achieve those improvements. To the best of our knowledge, there is no previous study dealing with the effect of graphene on the electrical and barrier properties of PHBV-based nanocomposites.

As it is widely recognized, *in situ* polymerization and solution casting are the most widely used routes to prepare polymer-graphene nanocomposites, mainly because of dispersion issues, since good results can be obtained through these methodologies.[13] However, both of them require a significant amount of organic solvents which are toxic and expensive and hence not convenient for industrial applications. On the contrary, although melt mixing is a more appropriate technique from an industrial view point, it leads to poorer dispersion of graphene into the polymer matrices. Despite of that, melt mixing can still be employed as a post-treatment after solution processing to develop graphene-based nanocomposites as previously described in different studies.[13,29,30] This strategy, which is a two steps process including the handling of liquids, has limited industrial scalability, although it provides an uniform dispersion of the filler avoiding the stacking or re-aggregation of the nanosheets.

Besides the mechanical reinforcing effect discussed above, graphene has a lamellar impermeable structure which can, in principle, should perform as a barrier element in polymer nanocomposites potentially decreasing gas and vapor permeability.[2] As previously reported, the incorporation of nanoplatelet-structured fillers into polymer matrices has demonstrated to be an effective strategy to generate high-barrier polymer films, mainly because of two factors, (i) increased tortuosity of the pathway leading to a reduction in the diffusion coefficient and (ii) reduction of the free volume by modification of the polymer chains mobility because of the adhesion between the filler and the polymer matrix.[31] Previous studies in the literature have corroborated the barrier effect of graphene-based nanofillers in polymer matrices.[12] For instance, reduced oxygen permeability of PLA-graphene nanocomposites has been reported showing reductions of up to 45%[31] or 68%.[24] Higher permeability reductions of up to 90%, were obtained in polyphenylene sulfide nanocomposites, although a high loading of the filler was required.[32]

A novel strategy that is being explored for the development of nanocomposites, is the solvent free processing method of the ball milling technique, which has demonstrated to be specially interesting for clay-based and carbon-based nanocomposites.[33–38] This technique is based on a high-energy milling, able to induce several mechanical and chemical changes in the materials. Moreover, graphene-based nanocomposites have also been synthesized by ball milling since this high-energy milling induces graphite delamination improving the final properties of the obtained materials.[37] An effective grafting of polystyrene

matrix (PS) onto the surface of graphene sheets using ball milling was reported, demonstrating, in this way, the effectiveness of the mechano-chemical character of this technique.[38] Furthermore, graphene nanoplateles were successfully incorporated into polyphenylene sulfide by ball milling with enhancement in mechanical, electrical, and barrier properties.[32] To the best of our knowledge, the high-energy ball milling technique (HEBM) has not been used up to date to develop PHBV-graphene nanocomposites or to show the effect of this processing technique in barrier properties. Because of this, the aim of the current study was to assess the use of this technique for the production of PHBV-graphene nanocomposites. As mentioned above this technique does not require the use of solvents or pretreatments of the filler, thus being a one-step process. The presence of oxygen functionalities in the graphene surface is very interesting from a chemical point of view, making it a suitable filler to create nanocomposites, as commented. Because of that, functionalized graphene sheets were used in an attempt to optimize the filler-matrix compatibilization.

In the first part of this study, functionalized graphene sheets were introduced into PHBV by means of HEBM. The morphology, thermal properties, and thermal stability of the obtained materials were evaluated and it was found that this technique led to a relatively good dispersion and distribution of the nanofiller within the polymer matrix, resulting in enhanced crystallinity because of the nucleating effect of the FGS. In the present work, the crystalline structure, mechanical, barrier and electrical properties as well as the biodegradability of the nanocomposites developed were evaluated, and related to their earlier morphological and thermal characterization.

MATERIALS AND METHODS

Materials

The bacterial polyhydroxyalkanoate grade was purchased from Goodfellow Cambridge Limited, UK, in pellet form (density 1.25 g/cm^3). The supplied material was a melt-processable semi-crystalline thermoplastic PHBV12 (polyhydroxybutyrate with 12 mol % of valerate and containing 10 wt % of the plasticizer citric ester) copolymer made by biological fermentation from renewable carbohydrate feedstocks. Prior to the ball milling process, the material was purified by dissolution in $CHCl_3$ and subsequent precipitation by drop-wise addition to an excess of methanol. The material, in this way, was transformed from pellet to powder form which was necessary for the ball milling process.

Functionalized graphene sheets (FGS) were synthesized by thermal reduction of graphite oxide at 1000°C for 30 s under air atmosphere. Briefly, graphite powder (purum powder < 0.1 mm, Sigma Aldrich) was dispersed in 20 mL of fuming nitric acid for 20 min; next, potassium chlorate (8 g) was slowly added over 1 h and the reaction mixture was stirred for 21 h at 0°C. Graphene produced through this method leads to the formation of single graphene layers or stacks of up to seven sheets with hydroxyl, carbonyl, and epoxy groups on their surface.[11] A full description of the synthesis and characterization of the FGS can be found elsewhere.[39]

Sample Preparation (HEBM)

FGS and PHBV powder were milled in the solid state in a Retsch (Germany) centrifugal ball mill (model PM100). The milling process was carried out in a cylindrical steel jar of 50 cm^3 with five steel balls of 10 mm of diameter. The rotation speed used was 650 rpm and the milling time was fixed to 60 min. In these experimental conditions, six series of composites PHBV–FGS with 0.1, 0.5, 1.0, 1.5, 2.0, and 3.0 wt % of FGS were prepared. An additional PHBV sample without filler to be taken as a reference was also milled in the same conditions. For the characterization, PHBV–FGS mixtures and the pure milled PHBV were molded in a hot press (Carver). To this aim the material was heated up to 175°C and kept at this temperature for 5 min. Subsequently, the material was hot pressed and cooled at room temperature giving rise to 250 ± 50 μm thick films. An illustration about the preparation of the PHBV/FGS nanocomposites can be seen in the first part of this work.

X-ray (XRD)

X-ray diffraction measurements (XRD) were performed with a Brucker diffractometer (equipped with a continuous scan attachment and a proportional counter) with Ni-filtered Cu Kα radiation ($\lambda = 1.54050$ Å). The samples were examined over the angular range of 2° to 40°.

Mass Transport Properties

Water barrier properties (sorption, diffusion) were evaluated using a microbalance SMS DVS Advantage-2 system. This system has a sensitivity of ±1.0 μg, and allows the measurements of mass changes because of sorption or desorption of vapor molecules. In this work the chosen method consisted in submitting the sample to pressure steps at constant temperature. The tests were conducted using water vapor in a nitrogen atmosphere at 30°C. The starting samples were dry, square films having a thickness of 200 μm and a side of 15 mm. The experimental protocol considered steps of relative humidity (RH) from 0% to 98%.

Oxygen Transmission Rate

The oxygen permeability coefficient was derived from oxygen transmission rate measurements recorded using an Oxtran 100 equipment (Modern Control, Minneapolis, MN, US). Experiments were carried out at 24°C and at 80% RH conditions. RH was generated by a built-in gas bubbler and was checked with a hygrometer placed at the exit of the detector. The samples were purged with nitrogen for a minimum of 20 h in the humidity equilibrated samples, prior to exposure to an oxygen flow of 10 mL/min. A 5 cm^2 sample area was measured by using an in-house developed mask. The measurements were done in duplicate.

Dynamic Mechanical Analysis (DMA)

Mechanical properties were evaluated using a DMA TAQ800. Measurements were conducted at the constant frequency (1 Hz) and amplitude (5 μm). The temperature was varied between −30°C and 140°C at 3°C/min.

Electrical Properties

The electrical conductivity was measured at room temperature with a Keithley 6517A electrometer unit in a two-probe

resistance measurement configuration controlled by a computer. The source delay for each point of measurement was about 3 s. For each measurement, the sample was placed between two copper electrodes. To enhance the electrical contact between the samples and the electrodes, metallization with Au was used. The metallization was conducted using an Agar Auto Sputter Coater (Agar Scientific Limited-UK-). The metallization time was 180 sec, for a metal deposition of about 22 nm. The electrical conductivity was measured in the voltage range −10 to 10 V. The electrical conductivity, σ (S/cm), of all the samples was obtained by using the basic equation:

$$\sigma = \frac{L}{\tau W}\frac{1}{R} = \frac{L}{\tau W}\frac{I_{\text{measured}}}{V_{\text{applied}}} \quad (1)$$

where $R(\Omega) = V_{\text{applied}}/I_{\text{measured}}$, τ (m), W (m), and L (m) are the resistance, the thickness, the width and the length of the specimens, respectively.

Biodisintegration in Composting Conditions

The biodesintegration of the samples under controlled composting condition was evaluated according to standard ISO 20200.[40] The solid waste was prepared by mixing 10% of compost (inoculum), 30% rabbit food, 10% starch, 5% sugar, 1% urea, 10% corn oil, and 40% sawdust. The inoculum used in the present study was mature compost supplied by Burés Profesional, SA (Girona, España). Prior to the mixing step, the compost was sieved through a 5 mm sieve. According to the standard, the water content was adjusted to 55wt % and kept at this level throughout the whole duration of the experiment by adding water periodically. The samples were cut into squares of 1.5 × 1.5 cm^2, buried inside the waste at a depth of approximately 6 cm and incubated at 58°C during 90 days inside polypropylene boxes. The specimens were individually sandwiched in between two stainless steel meshes, thus allowing full direct contact with the waste, while simplifying the extraction and labeling of the samples. In order to ensure aerobic conditions to take place, holes were performed on the boxes and, according to the standard, the waste was periodically stirred gently. The samples were extracted at different disintegration times (7, 15, 27, 41, 56, 69, 76, 83, and 90 days) washed with distilled water, dried at 40°C under vacuum for 24 h, and weighed. The disintegration degree was determined by normalizing the sample weight for every incubation time to its initial weight.

RESULTS AND DISCUSSION

Crystal Morphology of the Nanocomposites

In the previous part of this study,[41] DSC analysis under isothermal and nonisothermal conditions showed an influence of FGS incorporation on the kinetics and dynamics of PHBV crystallization. Specifically, the crystallization rate and the homogeneity of the crystals were altered and these effects were strongly dependent on the amount of FGS added to the polymer matrix. It was observed that addition of high concentrations of FGS somehow hindered the crystallization process, i.e. the increase in crystallinity was not as pronounced as with lower FGS contents but, at the same time, an acceleration of the crystallization process was observed. As a consequence, more defective or unstable crystals and a faster crystallization process were obtained when high FGS concentrations were used.

The crystal structure of the nanocomposite films was in the second part of this work studied by X-ray analysis. It has been previously reported that PHBV exhibits an isodimorphism phenomenon, and as a consequence the material could crystallize in either PHB unit cell or PHV unit cell, depending on the HV content. The transformation from the PHB lattice to the PHV lattice has been reported to occur at about 30 mol % HV.[42] However, Scandola *et al.*[43] reported that while for 34 mol % of HV, PHB crystalline phase was developed, and for 55 mol % of HV the X-ray diffraction spectra showed the pattern of the PHV crystalline phase, for 41 mol % of HV, PHB and PHV type crystals coexisted. It has also been previously reported that the reflection at $2\theta = 17°$ is associated with the (110) diffraction of PHB lattice, while that at $2\theta = 18°$ is associated with the (020) diffraction of PHV lattice.[44] Figure 1 shows the diffractograms of the different samples. The diffractogram of PHBV shows that this biopolyester is a semicrystalline material with the characteristic reflections from an orthorhombic cell.[2,42,45] It can be observed that there was no diffraction peak at $2\theta = 18°$ and, thus, only the typical PHB lattice was developed in the different materials. This result suggests that addition of graphene did not modify the crystal unit cell since the reflections for the nanocomposites appeared at the same diffraction angles than those from the neat polymer. In fact, the same spacing between planes were obtained for PHBV and its nanocomposites when applying Bragg's law (cf. Table I) suggesting that the parameters of PHBV unit cell were not influenced by FGS addition. Nevertheless, addition of FGS resulted in sharper peaks for the (020) and (110) PHBV reflections when compared to those of pure PHBV. This could be related with an increase in the crystallites lamella size, thus confirming that addition of these nanofillers promoted crystallization.[45] Scherrer equation [eq. (2)] was used to determine the crystallite size for the peak corresponding to the (020) reflection of PHBV and its nanocomposites.

$$L(\text{nm}) = \frac{K \cdot \lambda}{\beta \cdot \cos\theta} \quad (2)$$

where K is a dimensionless shape factor with a value close to unity, which is $K = 0.94$ for orthorhombic cell,[45] λ is the wavelength of the X-ray radiation which for CuKα radiation is 1.54Å, θ is the Bragg angle and β is the full width half maximum. From Table I it can be observed that the lamella size for the (020) reflection increased with the addition of FGS, confirming that addition of FGS effectively promoted the crystallization of PHBV, which is in agreement with previous works,[45] although the increase observed here was much more pronounced. A slight decrease in crystal lamella size was observed for high loadings. This is in agreement with the observations reported in the first part of this work[41] related to reduced crystallization at high loadings. Moreover, in order to evaluate how the addition of FGS affected the crystal growth, the ratio between the intensity of the peaks related to (020) and (110) crystal planes was calculated and can also be seen in Table I. An increase in the ratio was noticed with FGS addition, pointing out that the crystals grew preferentially in the direction of the

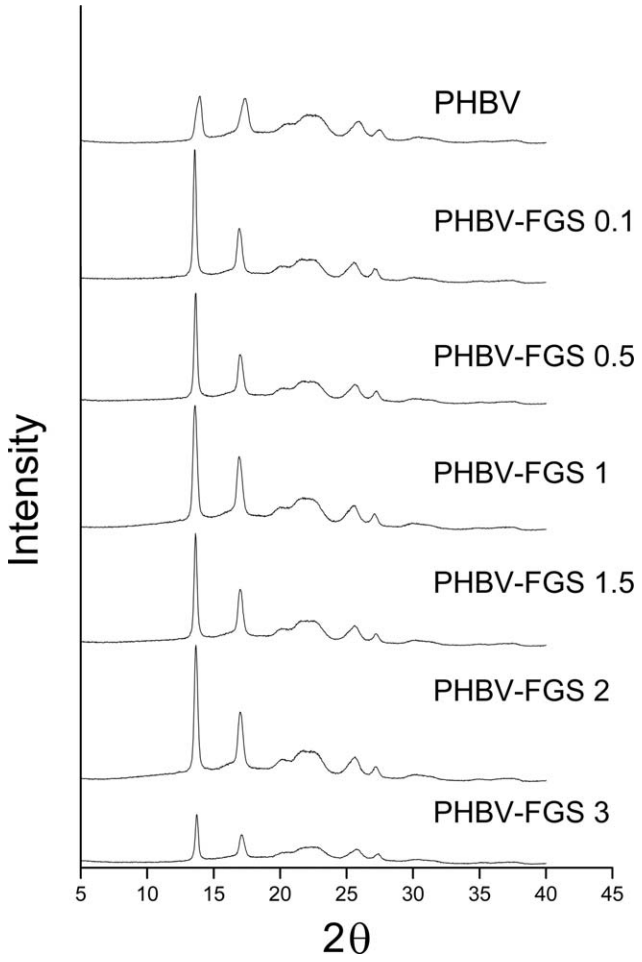

Figure 1. X-ray patterns of PHBV and its nanocomposites

(020) crystal plane, since an increase in the relative intensity of PHBV crystallite in a particular direction indicates that the PHBV crystals grow in a preferential orientation along that direction, as previously reported.[45]

Therefore, taking into account the DSC analysis performed in the previous work in combination with the X-ray analysis, it could be concluded that addition of FGS to the PHBV matrix did not alter the morphology of the crystalline unit cell, but had an effect on the kinetics and dynamics of PHBV crystallization, leading to an increased crystallinity content in the nanocomposites.

Mass Transport Properties

Graphene is considered a promising nanomaterial to promote gas or vapor barrier applications because perfect graphene sheets are able to block the diffusion of small molecules. A thorough revision about the use of graphene to improve barrier properties in polymer nanocomposites was carried out by Yoo *et al.*[12] However, although a broad range of polymers, graphene types, and processing methods for graphene-based nanocomposite development have been studied, no data were shown for PHBV nanocomposites nor for nanocomposites developed using ball milling. Although several works have reported about the incorporation of graphene into PHBV matrices,[2,28] to the best of our knowledge, the effect of this nanofiller on the transport properties of low molecular weight components through PHBV have not been previously investigated.

Mass transport properties such as water sorption and diffusion were evaluated for PHBV and PHBV-FGS 3.0 wt % nanocomposite. By measuring the normalized weight uptake over time, it is possible to infer the equilibrium concentration of sorbed water vapor, i.e. C_{eq} ($g_s/100g_p$), where g_s stands for grams of sorbed water vapor and g_p stands for grams of dry polymeric sample. Figure 2(a) reports the isotherms of water vapor sorption as a function of water activity (a_w). Similar water sorption isotherms were previously reported for PHB where a moderately hydrophobic character was assumed.[46] The hydrophobic character of the polymer was also reported for PHBV by others authors.[47] From the results, it can be seen that incorporation of FGS of 3 wt % had no effect on water sorption since no changes in the isotherms were observed when compared with this of the neat PHBV.

Moreover, by fitting the experimental data to the corresponding Fick's law [see eq. (3)], the diffusion coefficient, D (cm^2/s), can be calculated:

$$\frac{C_t}{C_{eq}} = 4\left(\frac{Dt}{\pi l^2}\right)^{1/2} = \left(\frac{16D}{\pi l^2}\right)^{1/2} t^{1/2} \quad (3)$$

where C_t and C_{eq} are the weight uptake for a given time t and at equilibrium, respectively, and l is the sample thickness.

Figure 2(b) shows the diffusion coefficients, D (cm^2/s), as a function of the equilibrium water uptake, C_{eq} ($g_s/100\ g_p$). The diffusion behavior was found to be very similar for both samples at each concentration with no effect on the water vapor diffusion coefficient upon addition of FGS. Recently published works, in which cellulose nanowhiskers or keratin were incorporated into PHBV, reported that only for filler loadings of 1 wt % there was a positive effect on water barrier properties. For higher filler loadings, no effect or even negative effects on water barrier properties were found.[1,48]

The oxygen permeability measured at 80% RH was also evaluated. Figure 3 displays the oxygen permeability of the PHBV and its nanocomposites. A decrease in oxygen permeability was observed for all the nanocomposites in comparison with the neat PHBV. Generally, it could be said that the oxygen barrier

Table I. Calculated Lamellar Spacing and Crystallite Sizes of PHBV and Its Nanocomposites with FGS

	d-Spacing (nm)	Crystallite size L_{020} (nm)	$I_{(020)}/I_{(110)}$
PHBV	0.64	16.3	1.1
PHBV-FGS 0.1%	0.65	30.8	2.3
PHBV-FGS 0.5%	0.65	30.4	2.1
PHBV-FGS 1%	0.65	29.9	1.6
PHBV-FGS 1.5%	0.65	30.1	1.9
PHBV-FGS 2%	0.65	26.5	1.9
PHBV-FGS 3%	0.65	27.4	1.6

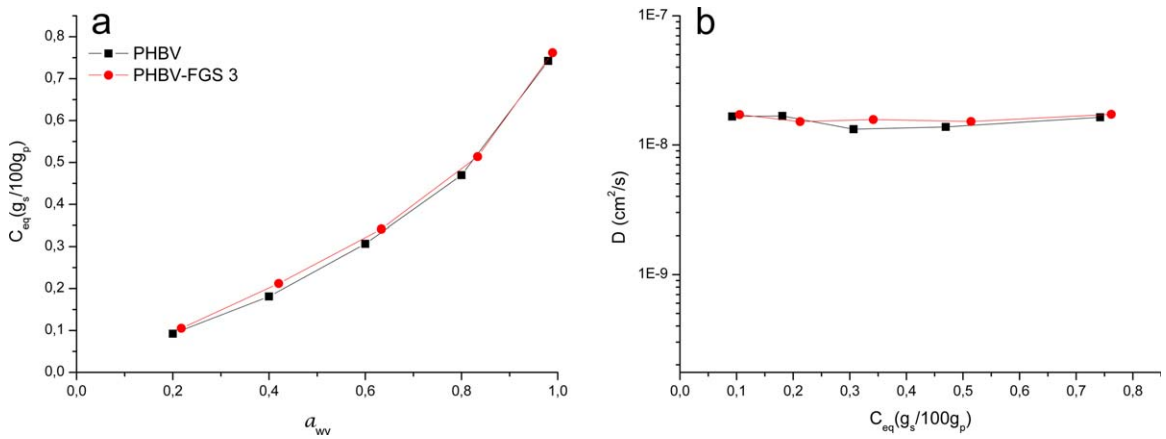

Figure 2. Sorption isotherms as function of water vapor activity (a_w) (a) and diffusion coefficients versus equilibrium sorbed water (C_{eq}) (b) of water vapor for pure PHBV and PHBV-FGS 3.0 wt % nanocomposites. [Color figure can be viewed in the online issue, which is available at wileyonlinelibrary.com.]

increases with the FGS content, reaching a maximum in barrier performance at 3 wt % filler loading exhibiting an oxygen permeability reduction of 41%. This barrier improvement is somewhere in line with the oxygen barrier improvements reported in the existing literature by other preparation methods (see the Introduction section), indicating that ball milling appears to be an alternative processing route to generate nanocomposites for these materials. Previous works have also reported a decrease in oxygen permeability when graphene nanoplatelets are used as filler.[24,32,46,47] It has been widely demonstrated that a good dispersion of the fillers and a good filler–matrix adhesion are crucial for improving barrier properties in polymer nanocomposites.[49] As observed in the morphological characterization of PHBV and its nanocomposites in the first part of this study[41] a good dispersion and distribution of the graphene lamellar structures were achieved. As a result, the improved barrier properties observed in the composites are here directly correlated with the favorably morphology observed in the results of the previous study. Moreover, as it is also widely known, an increase in crystallinity of semicrystalline biopolyesters has also been related to improved barrier properties mainly because of the tortuousity concept linked to the presence of the crystalline domains.[50–53] Addition of FGS into PHBV led to an increase in polymer crystallinity as measured by DSC in the first part of this study. Therefore, the increased oxygen permeability could also be ascribed to the increase in the crystalline fraction. In order to separate the effect of filler loading on the barrier performance from crystallinity alterations, the permeability drop across composition was divided by the crystallinity of the sample, to study, in relative terms, the impact of the filler in the barrier performance. This factor, which has been termed before as the filler efficiency barrier drop,[6] is gathered in Table II. From the results, an enlarged increased in permeability drop compared to the neat resin was observed as the FGS content increased except for the 0.5 and 1 wt % of FGS compositions. As observed, higher crystallinity was obtained for the latter two compositions if compared with for instance the 0.1 wt % FGS sample. Hence, the lower relative permeability drop for these two particular samples was directly ascribed to a lower blocking capacity per filler loading. The samples with 0.1 wt % and higher than 1 wt % FGS led to more efficiency of the filler per filler loading in terms of blocking permeation.

Dynamic Mechanical Analysis

In many current applications, polymer and polymer-nanocomposites are subjected to many temperature and frequency fluctuations. In order to evaluate the effect of graphene on temperature-dependent relaxation behavior of PHBV matrix, thermo-mechanical properties were evaluated in some of the samples developed. Figure 4 shows the storage modulus and tan δ, also known as loss factor, as a function of temperature as well as the storage modulus at 25°C and the maximum of tan δ which is related with the glass transition temperature of the nanocomposites (T_g). T_g values of the developed materials could not be discerned by a conventional method of T_g measurement by DSC. Nevertheless, the glass transition temperature measured by DMA generally increased with FGS addition. This trend is consistent with previous works where graphene or multiwalled carbon nanotubes (MWNT) were incorporated in PHBV.[2,45] The increase in T_g may be because of the restriction of the chain mobility within the polymer matrix upon addition of FGS. The neat PHBV exhibited a tan δ transition around 17°C,

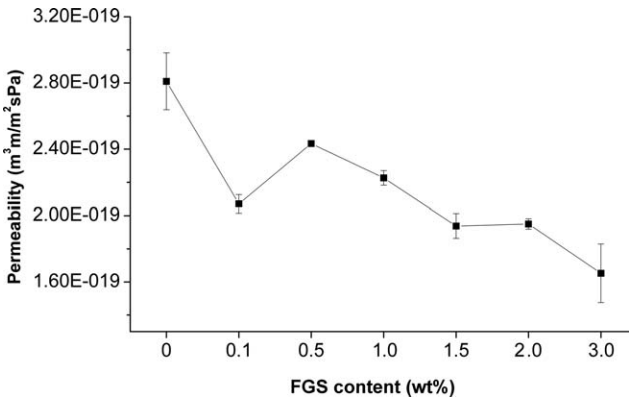

Figure 3. Oxygen permeability of pure PHBV and its nanocomposites with FGS.

Table II. Graphene Barrier Efficiency Data for PHBV and Its Nanocomposites

	Permeability drop (%)	Simple crystallinity[a](%X_c)	Filler barrier efficiency permeability drop(%)/ %crystallinity
PHBV	-	53.2	-
PHBV-FGS 0.1%	26.3	59.5	0.44
PHBV-FGS 0.5%	13.4	59.9	0.22
PHBV-FGS 1%	20.8	61.9	0.33
PHBV-FGS 1.5%	31.0	61.5	0.50
PHBV-FGS 2%	30.6	57.3	0.53
PHBV-FGS 3%	41.2	56.0	0.73

[a] Calculated in the first part of this work.[41]

which could be related to the glass transition of the amorphous PHBV molecules,[54] whereas for PHBV-FGS nanocomposites the glass transition temperatures were around, 21°C, 19°C, 22°C, and 24°C for 0.5, 1, 2, and 3 wt % respectively. In fact, at temperatures lower than T_g the loss factor for the pristine polymer was higher than for the nanocomposites. This means that high energy was dissipated, which could be mainly ascribed to internal frictions of polymer chains which, in turn, were related to increased mobility of those chains. The results also showed that the FGS nanofiller increased the storage modulus of the neat PHBV in the whole temperature span (cf. Figure 4). However, at 0.5 wt % filler content no effects were observed since no changes in the storage modulus curve were noticed. The reinforcing effect of graphene has been previously reported by several authors.[2,13–15,19,55] Although the storage modulus of nanocomposites was always higher than that for neat polymer, greater increases were observed at low temperatures ("glassy modulus") than those observed at temperatures above T_g ("rubbery modulus"). Evaluation of the storage modulus at 25°C was carried out and the same trend was noticed, i.e an increase from 2.1 to 2.8 GPa (enhancement of 35%) for neat PHBV and PHBV-FGS 3 wt %, respectively [cf. Figure 4(c)]. The same effects were observed for PHBV-graphene nanocomposites prepared through solution casting,[2] and also in PHBV-MWNT prepared by means of direct melt mixing.[45] In addition, previous works incorporating graphene into PLA have reported that the storage modulus increased when increasing the graphene content even at low filler loadings.[13] The homogeneous dispersion of nanofillers and filler–matrix interfacial interactions are important factors in the development of high-performance polymer materials, which are directly related with improvements in mechanical properties. A comparative study of highly and poorly dispersed graphene/epoxy nanocomposites revealed that the highly dispersed graphene fillers are more efficient than the aggregated ones in transferring the applied load.[56] In view of the results, it could be generally stated that a good dispersion and filler–matrix adhesion were attained, being this premise supported by the oxygen barrier data.

Electrical Properties

A good dispersion of conductive carbonaceous materials, such as carbon nanotubes, graphite, graphene, and/or its derivatives into polymeric matrices, is widely known to improve the electrical properties of the final composite materials. Figure 5 shows the electrical conductivities of PHBV and its nanocomposites. Neat PHBV is electrically insulating with a low conductivity ($\sim 10^{-13}$ S/cm). Nevertheless, the addition of conducting FGS nanofillers significantly increased the conductivity of the materials. The S-shaped curves indicate that the nanocomposites exhibited a typical percolation transition from an insulator to a semiconductor.[37,38] The percolation theory describes the behavior of connected fillers in a randomly dispersed system. In this case, the connected fillers were FGS. An analytical model has been previously proposed, based on the Fermi–Dirac distribution, to describe the critical insulator to conductor transition:[33]

$$\log(\sigma_c) = \log(\sigma_f) + \frac{\log(\sigma_p/\sigma_f)}{(1+\exp(t(\varphi-\varphi_c)))} \quad (4)$$

where σ_c, σ_f, and σ_p are the composite, filler, and polymer conductivities, respectively, ϕ is the FGS mass fraction, and t is an empirical parameter that leads to the change in conductivity at the percolation threshold ϕ_c. By assuming a constant value for σ_f and σ_p, from eq. (4), the best fitted values of ϕ_c and t were obtained. Thus, the percolation threshold value of nanocomposites was calculated to be about ~0.8 wt % (~ 0.3 vol %). It is thought that the low FGS content for electrical percolation threshold is related with the high aspect ratio of FGS and also to a homogeneously and well-dispersed nanofiller into the polymer matrix, as observed by SEM and TEM (see the previous study),[41] which allowed the conductive filler to form an extensive network of connected paths through the insulating matrix. Room temperature conductivities (RTC) of up to ~0.1 S cm^{-1} were achieved for samples with 3 wt % filler loading, sufficient for many electrical applications.

Biodisintregration in Composting Conditions

As a biodegradable material, PHA's are susceptible to be degraded under natural environmental conditions upon disposal. In order to evaluate the effect of graphene-based fillers addition into PHBV on its biodegradation, bio-disintegration of the PHBV and its nanocomposites were studied in composting conditions. Figure 6 shows the bio-disintegration (as percentage of weight loss) as a function of time. As observed, despite the fact that some studies about the cyto- and genotoxicity of the graphene have been recently published,[57,58] no detrimental effect

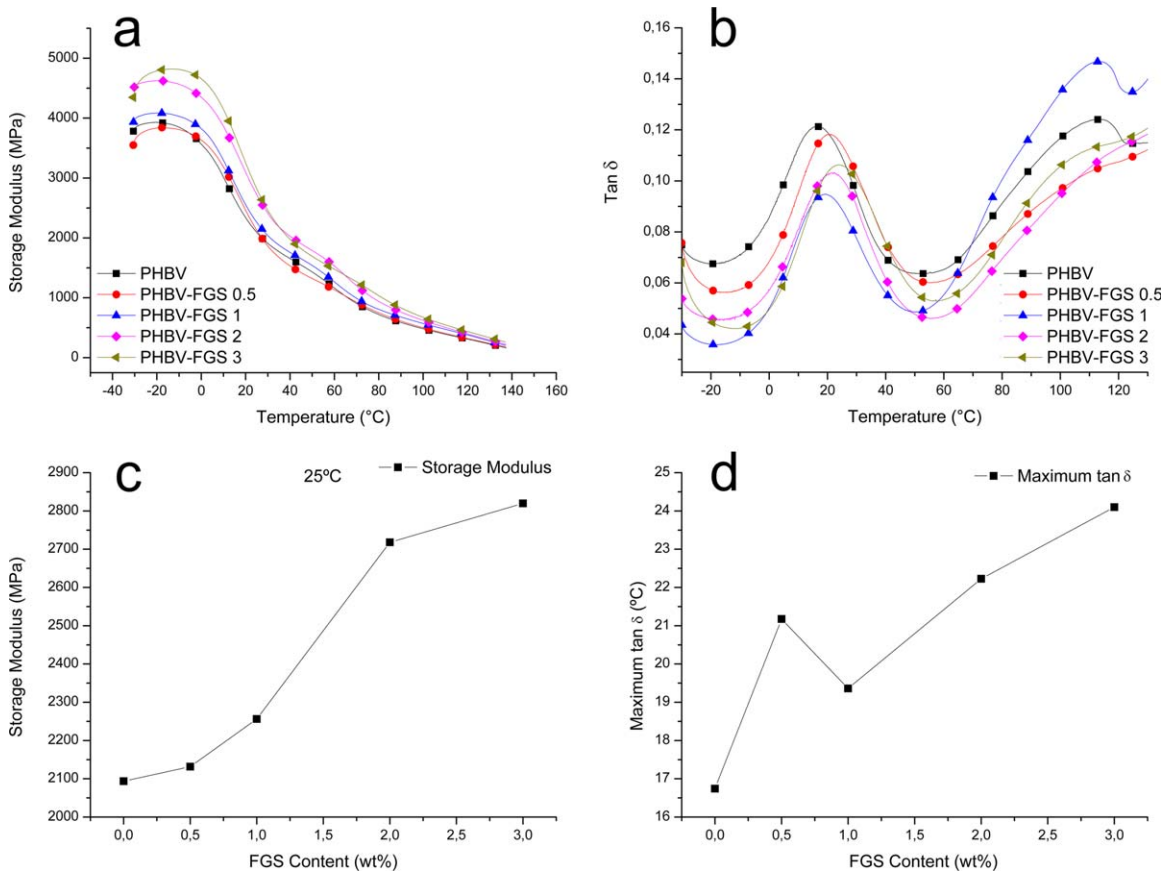

Figure 4. Dynamo-mechanical analysis of PHBV and its nanocomposites. Storage modulus (a) and tan δ (b) versus temperature, storage modulus at 25°C (c) and maximum of tan δ (d). [Color figure can be viewed in the online issue, which is available at wileyonlinelibrary.com.]

upon addition of FGS at different concentrations on the biodegradation process were observed but rather the opposite. Thus, it is worth mentioning that an acceleration of the process was mostly observed for the samples loaded with the carbonaceous material since higher weight losses were appreciated at determined tested times for the nanocomposites. Moreover, as observed from Figure 6, the sample with the highest graphene loading degraded faster. Specifically, while the weight loss of pure PHBV was 33% after 56 days of compost incubation, weight losses of 60% and 94.6% were observed for the samples loaded with 1 and 3 wt %, respectively.

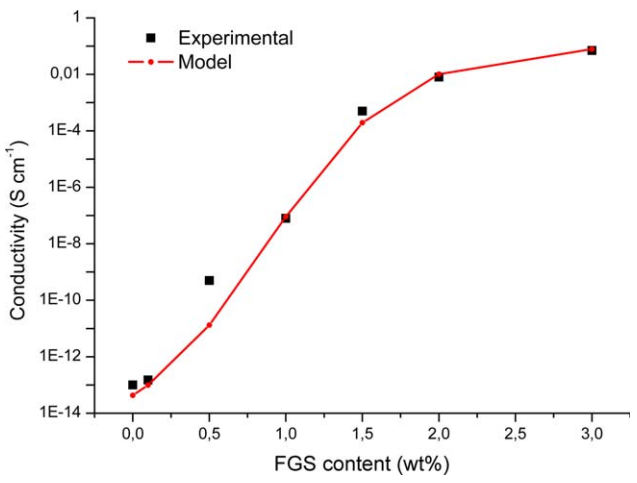

Figure 5. Experimental and calculated electrical conductivity versus filler loading for PHBV-FGS nanocomposites. [Color figure can be viewed in the online issue, which is available at wileyonlinelibrary.com.]

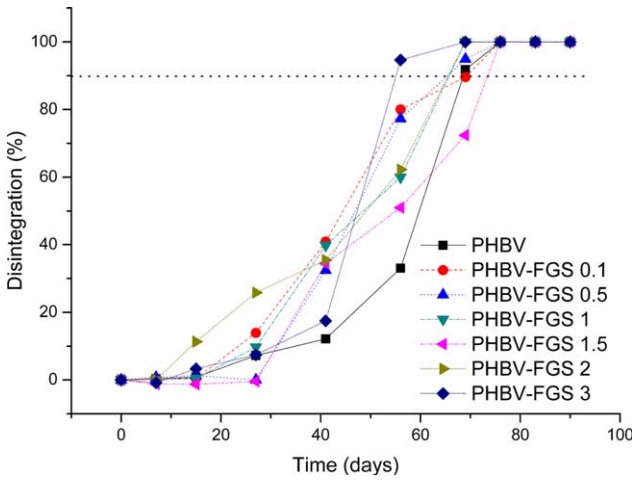

Figure 6. Loss in weight as a result of the biodegradation of PHBV and PHBV-FGS nanocomposites in composting conditions for up to 90 days. [Color figure can be viewed in the online issue, which is available at wileyonlinelibrary.com.]

CONCLUSIONS

In this article a PHBV polymer containing functionalized graphene sheets (FGS) obtained by ball milling were characterized in terms of physical properties to assess its applicability as barrier, mechanical, and electrically conductive materials. The resulted nanocomposites showed improved crystallinity and physical properties. X-ray diffraction, in combination with isothermal and nonisothermal crystallization studies performed in the first part of this work, indicated that addition of FGS did not modify the crystal morphology of the PHBV matrix but led to an increase in crystallinity content. A reduction in oxygen permeability was observed upon addition of FGS which was ascribed most likely to the combined effect of the highly dispersed and distributed laminar filler and increased crystallinity. However, no effects were observed in terms of water vapor mass transport properties across the composition range study. Addition of FGS resulted in an increase in the storage modulus mainly because of the reinforcing effect of FGS homogeneously dispersed and distributed in the PHBV matrix. The electrical percolation threshold of PHBV-FGS nanocomposites was attained at $\sim$ 0.3 vol %, increasing the PHBV matrix conductivity 12 log units to reach a room temperature conductivity of up to $\sim$0.1 S/cm. Finally, acceleration of the bio-disintegration process of the PHBV was observed upon addition of FGS. This study proves that the ball milling technique can be successfully applied to generate gas barrier and mechanically reinforced nanocomposites with enhanced conductivity of interest in various application fields such as barrier and intelligent packaging.

ACKNOWLEDGMENTS

J. Ambrosio-Martín would like to thank the Spanish Ministry of Economy and Competitiveness for the FPI grant BES-2010-038203. M.J. Fabra is recipient of a "Juan de la Cierva" contract from the Spanish Ministry of Economy and Competitiveness. The authors acknowledge financial support from the MINECO (MAT2012- 38947-C02-01 project) and the EU FP7 ECOBIOCAP project.

REFERENCES

1. Martínez-Sanz, M.; Villano, M.; Oliveira, C.; Albuquerque, M. G. E.; Majone, M.; Reis, M.; Lopez-Rubio, A.; Lagaron, J. M. *New Biotechnol.* **2014**, *31*, 364.
2. Sridhar, V.; Lee, I.; Chun, H. H.; Park, H. *Express Polym. Lett.* **2013**, *7*, 320.
3. Lai, M.; Li, J.; Yang, J.; Liu, J.; Tong, X.; Cheng, H. *Polym. Int.* **2004**, *53*, 1479.
4. Ten, E.; Jiang, L.; Wolcott, M. P. *Carbohydr. Polym.* **2012**, *90*, 541.
5. Ublekov, F.; Baldrian, J.; Nedkov, E. *J. Polym. Sci. B Polym. Phys.* **2009**, *47*, 751.
6. Sanchez-Garcia, M. D.; Lagaron, J. M. *J. Appl. Polym. Sci.* **2010**, *118*, 188.
7. Martínez-Sanz, M.; Vicente, A. A.; Gontard, N.; Lopez-Rubio, A.; Lagaron, J. M. *Cellulose* **2014**.
8. Yu, H. Y.; Qin, Z. Y.; Yan, C. F.; Yao, J. M. *Chem. Eng.* **2014**, *2*, 875.
9. Yu, H.; Yan, C.; Yao, J. *RSC Adv.* **2014**, *4*, 59792.
10. Marques, P. A. A. P.; Gonçalves, G.; Cruz, S.; Almeida, N.; Singh, M. K.; Grácio, J.; Suosa, A. C. M. In Advances in Nanocomposite Technology; Hassim, A., Ed.; InTech: Rijeka (Croatia), **2011**; Chapter 11.
11. Schniepp, H. C.; Li, J. L.; McAllister, M. J.; Sai, H.; Herrera-Alonson, M.; Adamson, D. H.; Prud'homme, R. K.; Car, R.; Seville, D. A.; Aksay, I. A. *J. Phys. Chem. B* **2006**, *110*, 8535.
12. Yoo, B. M.; Shin, H. J.; Yoon, H. W.; Park, H. B. *J. Appl. Polym. Sci.* **2014**, 131.
13. Bao, C.; Song, L.; Xing, W.; Yuan, B.; Wilkie, C. A.; Huang, J.; Guo, Y.; Hu, Y. *J. Mater. Chem.* **2012**, *22*, 6088.
14. Wang, J.; Wang, X.; Xu, C.; Zhang, M.; Shang, X. *Polym. Int.* **2011**, *60*, 816.
15. El Achaby, M.; Qaiss, A. *Mater. Des.* **2013**, *44*, 81.
16. Ding, P.; Su, S.; Song, N.; Tang, S.; Liu, Y.; Shi, L. *Carbon* **2014**, *66*, 576.
17. Stankovich, S.; Dikin, D. A.; Dommett, G. H. B.; Kohlhaas, K. M.; Zimney, E. J.; Stach, E. A.; Piner, R. D.; Nguyen, S. T.; Ruoff, R. S. *Nature* **2006**, *442*, 282.
18. Fang, M.; Wang, K.; Lu, H.; Yang, Y.; Nutt, S. *J. Mater. Chem.* **2009**, *19*, 7098.
19. Zhao, X.; Zhang, Q.; Chen, D.; Lu, P. *Macromolecules* **2010**, *43*, 2357.
20. Salavagione, H. J.; Martínez, G.; Gómez, M. A. *J. Mater. Chem.* **2009**, *19*, 5027.
21. Kuila, T.; Bose, S.; Mishra, A. K.; Khanra, P.; Kim, N. H.; Lee, J. H. *Polym. Test.* **2012**, *31*, 31.
22. De C.. Fim,; F.; Basso,; N. R. S.; Graebin,; A. P.; Azambuja,; D. S.; Galland,; G. B. *J. Appl. Polym. Sci.* **2013**, *128*, 2630.
23. Kim, I. H.; Jeong, Y. G. *J. Polym. Sci. B Polym. Phys.* **2010**, *48*, 850.
24. Pinto, A. M.; Cabral, J.; Tanaka, D. A. P.; Mendes, A. M.; Magalhães, F. D. *Polym. Int.* **2013**, *62*, 33.
25. Shen, Y.; Jing, T.; Ren, W.; Zhang, J.; Jiang, Z. G.; Yu, Z. Z.; Dasari, A. *Compos. Sci. Technol.* **2012**, *72*, 1430.
26. Li, W.; Xu, Z.; Chen, L.; Shan, M.; Tian, X.; Yang, C.; Lv, H.; Qian, X. *Chem. Eng. J. (Lausanne)* **2014**, *237*, 291.
27. Yang, J. H.; Lin, S. H.; Lee, Y. D. *J. Mater. Chem.* **2012**, *22*, 10805.
28. Wang, B. J.; Zhang, Y. J.; Zhang, J. Q.; Gou, Q. T.; Wang, Z. B.; Chen, P.; Gu, Q. *Chin. J. Polym. Sci. (English Edition)* **2013**, *31*, 670.
29. Song, P.; Cao, Z.; Cai, Y.; Zhao, L.; Fang, Z.; Fu, S. *Polymer* **2011**, *52*, 4001.
30. Song, P.; Liu, L.; Fu, S.; Yu, Y.; Jin, C.; Wu, Q.; Zhang, Y.; Li, Q. *Nanotechnology* **2013**, 24,.
31. Huang, H. D.; Ren, P. G.; Xu, J. Z.; Xu, L.; Zhong, G. J.; Hsiao, B. S.; Li, Z. M. *J. Membr. Sci.* **2014**, *464*, 110.
32. Jiang, X.; Drzal, L. T. *J. Power Sources* **2012**, *218*, 297.
33. Gorrasi, G.; Di Lieto, R.; Patimo, G.; De Pasquale, S.; Sorrentino, A. *Polymer* **2011**, *52*, 1124.

34. Gorrasi, G.; Sarno, M.; Di Bartolomeo, A.; Sannino, D.; Ciambelli, P.; Vittoria, V. *J. Polym. Sci. B Polym. Phys.* **2007**, *45*, 597.
35. Vertuccio, L.; Gorrasi, G.; Sorrentino, A.; Vittoria, V. *Carbohydr. Polym.* **2009**, *75*, 172.
36. Perrin-Sarazin, F.; Sepehr, M.; Bouaricha, S.; Denault, J. *Polym. Eng. Sci.* **2009**, *49*, 651.
37. Wu, H.; Zhao, W.; Chen, G. *J. Appl. Polym. Sci.* **2012**, *125*, 3899.
38. Wu, H.; Zhao, W.; Hu, H.; Chen, G. *J. Mater. Chem.* **2011**, *21*, 8626.
39. Verdejo, R.; Barroso-Bujans, F.; Rodriguez-Perez, M. A.; De Saja, J. A.; Lopez-Manchado, M. A. *J. Mater. Chem.* **2008**, *18*, 2221.
40. ISO Standard 20200:2004. "Determination of the degree of disintegration of plastic materials under simulated composting conditions in a laboratory-scale test". International Organization for Standardization.
41. Ambrosio-Martín, J.; Gorrasi, G.; Lopez-Rubio, A.; Fabra, M. J.; Cabedo, L.; López-Manchado, M. A.; Lagaron, J. M. *J. Appl. Polym. Sci.* **2015**.
42. Kunioka, M.; Tamaki, A.; Doi, Y. *Macromolecules* **1989**, *22*, 694.
43. Scandola, M.; Ceccorulli, G.; Pizzoli, M.; Gazzano, M. *Macromolecules* **1992**, *25*, 1405.
44. Shan, G. F.; Gong, X.; Chen, W. P.; Chen, L.; Zhu, M. F. *Colloid Polym. Sci.* **2011**, *289*, 1005.
45. Vidhate, S.; Innocentini-Mei, L.; D'Souza, N. A. *Polym. Eng. Sci.* **2012**, *52*, 1367.
46. Kalaitzidou, K.; Fukushima, H.; Drzal, L. T. *Carbon* **2007**, *45*, 1446.
47. Potts, J. R.; Dreyer, D. R.; Bielawski, C. W.; Ruoff, R. S. *Polymer* **2011**, *52*, 5.
48. Pardo-Ibáñez, P.; Lopez-Rubio, A.; Martínez-Sanz, M.; Cabedo, L.; Lagaron, J. M. *J. Appl. Polym. Sci.* **2014**, 131.
49. Sorrentino, A.; Gorrasi, G.; Vittoria, V. In Environmental Silicate Nano-Biocomposites; Avérous, L.; Pollet, E., Eds.; Springer: London, **2012**; Chapter 9.
50. Colomines, G.; Ducruet, V.; Courgneau, Ć.; Guinault, A.; Domenek, S. *Polym. Int.* **2010**, *59*, 818.
51. Kanehashi, S.; Kusakabe, A.; Sato, S.; Nagai, K. *J. Membr. Sci.* **2010**, *365*, 40.
52. Tsuji, H.; Okino, R.; Daimon, H.; Fujie, K. *J. Appl. Polym. Sci.* **2006**, *99*, 2245.
53. Komatsuka, T.; Kusakabe, A.; Nagai, K. *Desalination* **2008**, *234*, 212.
54. Cimmino, S.; Iodice, P.; Silvestre, C.; Karasz, F. E. *J. Appl. Polym. Sci.* **2000**, *75*, 746.
55. Zhao, J.; Wang, X.; Zhou, W.; Zhi, E.; Zhang, W.; Ji, J. *J. Appl. Polym. Sci.* **2013**, *130*, 3212.
56. Tang, L. C.; Wan, Y. J.; Yan, D.; Pei, Y. B.; Zhao, L.; Li, Y. B.; Wu, L. B.; Jiang, J. X.; Lai, G. Q. *Carbon* **2013**, *60*, 16.
57. Akhavan, O.; Ghaderi, E.; Akhavan, A. *Biomaterials* **2012**, *33*, 8017.
58. Akhavan, O.; Ghaderi, E.; Emamy, H.; Akhavan, F. *Carbon* **2013**, *54*, 419.